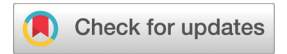
Nanoscale



PAPER

View Article Online
View Journal | View Issue



Cite this: Nanoscale, 2019, 11, 11808

A chemoinformatics approach for the characterization of hybrid nanomaterials: safer and efficient design perspective?

In this study, photocatalytic properties and in vitro cytotoxicity of 29 TiO2-based multi-component nanomaterials (i.e., hybrids of more than two composition types of nanoparticles) were evaluated using a combination of the experimental testing and supervised machine learning modeling. TiO2-based multi-component nanomaterials with metal clusters of silver, and their mixtures with gold, palladium, and platinum were successfully synthesized. Two activities, photocatalytic activity and cytotoxicity, were studied. A novel cheminformatic approach was developed and applied for the computational representation of the photocatalytic activity and cytotoxicity effect. In this approach, features of investigated TiO2-based hybrid nanomaterials were reflected by a series of novel additive descriptors for hybrid and hybrid nanostructures (denoted as "hybrid nanosctructure descriptors"). These descriptors are based on quantum chemical calculations and the Smoluchowski equation. The obtained experimental data and calculated hybrid-nanostructure descriptors were used to develop novel predictive Quantitative Structure-Activity Relationship computational models (called "nano-QSAR_{mix}"). The proposed modeling approach is an initial step in the understanding of the relationships between physicochemical properties of hybrid nanoparticles, their toxicity, and photochemical activity under UV-vis irradiation. Acquired knowledge supports the safe-by-design approaches relevant to the development of efficient hybrid nanomaterials with reduced hazardous effects.

Received 6th February 2019 Accepted 22nd May 2019 DOI: 10.1039/c9nr01162e

rsc.li/nanoscale

1. Introduction

Pristine titania nanoparticles (TiO₂ NPs) have been widely studied because of their promising applications as environmentally friendly nanomaterials. TiO₂ NPs could be used for photodegradation of organic pollutants, photocatalytic splitting of water for hydrogen production, conversion of solar energy into electric energy, and reduction of CO₂ in organic fuels. Notwithstanding the rising interest, the homogeneous

TiO2 NPs demonstrate photocatalytic activity only at UV irradiation that only is a 5% share of the natural solar energy. Propagating the usability of TiO₂ NPs to solar light may lead to the expansion of nanomaterial's applicability in the fields of nanoscience and technology. One of the potential ways to improve photocatalytic properties of TiO2 NPs in visible light is to design modified hybrid/multicomponent TiO2-based nanomaterials that contain specific surface/structure modification and/or functionalization (so-called 2nd generation NPs).¹⁻⁴ At the same time, these new physicochemical properties of modified TiO2 NPs may result in increased hazardous effects to the human body or to the environment. To guarantee that only safe TiO2-based nanomaterials would be further synthesized, 5,6 safer-by-design approaches should be developed and applied. To date, there are no standardized methods for the evaluation of potential hazard effects of hybrid nanomaterials. The literature survey indicates that the amount of experimental data grows every year. 7 In order to effectively interpret and transfer the experimental data, research methods could include computational modeling, enabling the relationships between nanomaterials' physicochemical characteristics and their hazard (safety) profiles.²

^aLaboratory of Environmental Chemometrics, Faculty of Chemistry, University of Gdansk, Wita Stwosza 63, 80-308 Gdansk, Poland.

 $[\]hbox{\it E-mail: tomasz.puzyn@ug.edu.pl, mikolajczyk@qsar.eu.org}$

^bDepartment of Environmental Analytics, Faculty of Chemistry, University of Gdansk, Wita Stwosza 63, 80-308 Gdansk, Poland

^cDepartment of Computer Science, Dartmouth College, 6211 Hinman, Hanover, New Hampshire 03755, USA

^dDepartment of Environmental Technology, Faculty of Chemistry, University of Gdansk, Wita Stwosza 63, 80-308 Gdansk, Poland

^eDepartment of Coatings and Polymeric Materials, North Dakota State University, NDSU Dept 2760, P.O. Box 6050, Fargo, ND 58108, USA

[†]Electronic supplementary information (ESI) available. See DOI: 10.1039/c9nr01162e

Nanoscale

One of the best time-efficient computational methods is a Quantitative Structure-Activity/Property Relationship (QSAR/ QSPR) approach.8 During the last ten years, various nanoparticles' properties have been modeled and predicted using this approach (known as "nano-QSAR/QSPR models"). The term "nano-QSAR" refers to the search of quantitative links between features of nanoparticles and target activity. Structural features are typically represented by a variety of numeric parameters (also known as "descriptors"). 1,4,8-11 The successful application of the Nano-OSAR/OSPR methodology has been already demonstrated for homogeneous NPs, such as metal oxides, silver clusters, carbon nanotubes and fullerenes. For example Luan et al. 12 applied computational modeling to describe the cytotoxicity of 41 pairs of metal/metal oxide NPs against several mammalian cell lines, based on the chemical composition of nanoparticles, size, conditions under which the size was measured, and shape. While Kleandrova et al. 13,14 presented QSTR-perturbation models to simultaneously probe ecotoxicity and cytotoxicity of 5520 NP pairs under different experimental conditions, including diverse measures of toxicities (CC₅₀, EC₅₀, IC₅₀, TC₅₀, LC₅₀), compositions, sizes and conditions to measure those sizes, shapes, times during which the biological targets were exposed to NPs, and coating agents. Chemoinformatic methods, including Nano-QSAR/QSPR models, have been also applied to carbon nanomaterials (CNTs) as predictive nanotoxicological tools that at the same time have allowed the classification with greater clarity of their toxic impact on human and environmental health. 15-18 For instance, recently, Gonzáles-Díaz et al. 15 have applied artificial neural network (ANN) classification models based on fractal SEM nanodescriptors for predicting the mitochondrial nanotoxicity on F0-ATPase subunit inhibition (ATP-hydrolysis inhibition) induced by CNTs. 17 Another vacancy quantitative structure-binding relationship (V-QSBR) model was developed for the prediction of the strength of docking interactions between

CNT nanotubes with a specific topological vacancy and

hVDAC1.¹⁸ Thus a series of specific descriptors for nanoparticles were ultimately developed, but the majority of currently available nano-descriptors are unable to reflect the structural complexity of hybrid nanoparticles. 1,4,8-11 This makes nano-QSAR modeling of hybrid TiO2-based nanomaterials a challenging task, as no proven modeling methodology is available.

This paper reports the development schema for predictive nano-QSAR modeling of the photocatalysis and cytotoxicity for hybrid TiO2-based nanomaterials (so called here nano-QSAR_{mix}). The ultimate aim of this project is to develop efficient TiO₂ photocatalysts with reduced cytotoxicity against eukaryotic cells. For this purpose, we investigated photocatalytic and cytotoxic effects of TiO₂-supported hybrid nanomaterials using a combination of experimental and computational techniques. Here we present a quantitative description of the photocatalytic activity in visible and UV-visible light and discuss the cytotoxicity against Chinese hamster ovary (CHO-K1) with the focus on concentration-dependent effects (Fig. 1).

2. Materials and methods

Preparation and characterization of hybrid/TiO2-based 2.1 nanomaterials

A set of 29 TiO2-based nanomaterials was synthesized by the sol-gel method. TiO2 NPs modified with Au, Ag, Pt and Pd nanoclusters (further denoted as Memix-TiO2) were prepared by the hydrolysis reaction of titanium isopropoxide (TIP) with water. In the first step, 25 cm3 TIP was dispersed in 25 cm3 ethanol at room temperature followed by 30 min solution mixing. After that, 14.2 cm3 of water was added to the alkoxide solution and a white precipitate was formed. Finally, 0.1 or 0.5mol% of either HAuCl₄, K₂PtCl₄, or PdCl₂, and 0.1, 0.5, 1.5, 2.5, or 4.5mol% of AgNO3 were dissolved in deionized water

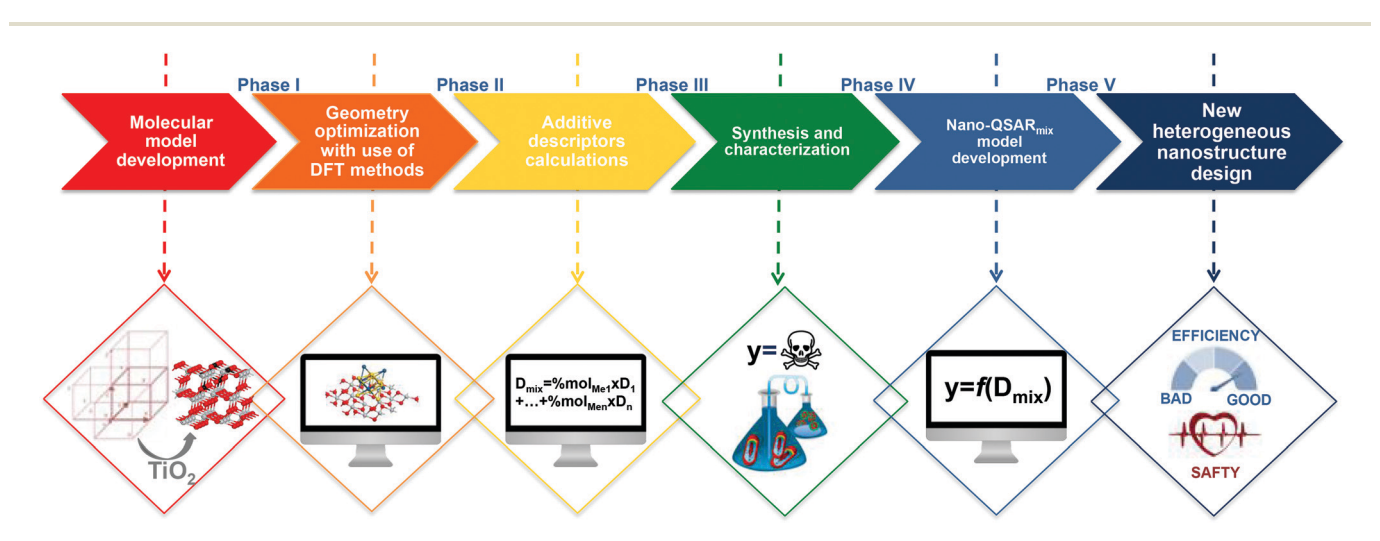


Fig. 1 The general schema of the proposed chemoinformatics-supported modeling strategy for hybrid nanomaterials. Term DFT here denotes Density Functional Theory.

Paper Nanoscale

and mixed with TiO_2 gel for 1 h. All the samples were obtained by the sequential addition of metal precursors to the TiO_2 gel. The obtained photocatalysts were dried at 80 °C and then calcined in air at 400 °C for 3 h. To see more technical details, please refer to the ESI (ESI, Table S1†).

2.1.1 Measurement of photocatalytic activity under visible light and UV-vis light. The photocatalytic activity of prepared hybrid TiO₂-based samples was estimated by the decomposition rate of a 0.21 mM phenol aqueous solution in the presence of visible UV-vis radiation. The aqueous phase contained 125 mg of the photocatalyst, 24 cm³ of deionized water and 1 cm^3 of phenol (Co = 500 mg dm⁻³). The prepared suspension was stirred and aerated in the dark, and the content of the reactor was then photo-irradiated with a 1000 W xenon lamp (Oriel). The optical path included a water filter and a glass filter (GG 420) that blocked wavelengths shorter than 420 nm. The phenol concentration was estimated by a colorimetric method using a UV-vis spectrophotometer (DU-7, Beckman). The photocatalytic activity of Memix-TiO2 nanoparticles was determined in the process of cleaning volatile organic compounds (VOC) from air under 25 mixed LEDs (5 LEDs, λ_{max} = 375 nm and 20 LEDs, λ_{max} = 415 nm) as the irradiation source. Toluene (Co = 200 ppm) was used as a model air contaminant. The suspension of the photocatalyst in water was loaded as a thick film onto a glass plate using the painting technique and subsequently dried. A flat stainless-steel reactor ($V = 30 \text{ cm}^3$) was equipped with a quartz window, two valves, and a septum. After the valves were closed, the reactor was kept in the dark for 15 min and the contents of the reactor were photoirradiated. The toluene concentration in the gas phase was chromatography measured using gas (Clarus 500, PerkinElmer).

2.1.2 Measurement of cytotoxicity. The cytotoxicity of the Me_{mix}-TiO₂ was experimentally tested using epithelial cells obtained from Chinese hamster ovary (CHO-K1 cell line, ATCC® CCL-61TM). For the experiment, investigated nanomaterials were prepared by grinding the powder for 5 min, then dissolved in a cell medium to a concentration of 1 mg mL⁻¹ (F12 medium supplemented with 2 mM L-glutamine, 1% antibiotic solution (penicillin/streptomycin) and 10% heat-inactivated FBS with 0.1% Pluronic added to prevent aggregation/agglomeration, and then sonicated in a water bath for 30 min at 37 °C. Cell viability was tested using a colorimetric assay with the WST-8 reagent. For the cytotoxicity assays, cells were seeded in 24-well plates at an initial density of 1 × 10⁵ cells per mL of culture medium and incubated for 24 h. Cells were exposed to nine different concentrations of NPs (from 300 to 1.56 $\mu g\ mL^{-1}$) for 24 h. Next, the WST-8 reagent was added and incubated for 2 h. As Au NPs absorb light in the visible spectrum, the plates were centrifuged to avoid interference with the assay. Finally, 100 µl of the medium from each well was transferred to a respective well in a 96-well plate, and the absorbance at 450 nm was measured in the plate reader. Cell viability was calculated as the percentage of the viability of exposed cells vs. controls. Concentration-response curves were fitted using the nonlinear

least-squares method employing the logistic model of the relationship between cell viability and the tested concentrations. The final values of the cytotoxicity were expressed as the logarithm of 50% inhibition of the cell viability (pEC $_{50}$). Calculations were carried out with the R programming language. ³²

2.2 Quantum-chemical calculations

To characterize hybrid TiO2-based nanomaterials computationally, a series of quantum-mechanical (QM) properties (viz. basic descriptors) were calculated.³³ The calculations of basic quantum-chemical descriptors were performed in the framework of Density Functional Theory (DFT) using the Gaussian 09 package and Vienna ab initio Simulation Package (VASP).34-36 The calculations were conducted as a two-step protocol: (i) the first step included investigation of $5 \times 5 \times 5$ Å metal clusters in a gas phase using the B3LYP functional and LANL2DZ basis set implemented into Gaussian 09 and (ii) solid state systems of Memix-TiO2, using the plane-wave based method in VASP, implementing spin-polarized DFT and the generalized gradient approximation (GGA) by Perdew-Burke-Ernzerhof (PBE) with an intra-site Coulomb interactions between Ti-3d electrons in Dudarev's approach, so-called PBE+U.^{37,38} The core electrons for Au-[Xe]4f,¹⁴ O-1s² and Ti-[Ne]3s2 were described by projector augmented wave potential (PAW). As a result, an energy of the highest occupied molecular orbital (E_{HOMO}) , energy of the lowest unoccupied molecular orbital (E_{LUMO}), ionization potential (IP), electron affinity (A), absolute electronegativity (μ) , absolute hardness (η) , total energy of the system (E_{tot}) and adsorption energy of metals $(E_{\rm ads})$ were calculated (ESI, Table S5†). As stated above, the conventional descriptors derived from quantum-mechanical calculations can be adapted to adequately represent surface-modified metal oxide nanoparticles.4 Basic quantum chemical descriptors were unable to reflect either the variety of noble metal concentrations or synergistic effects of different metals in a hybrid mixture. At the same time, the quantum-chemical calculations of large and complex nano-sized systems are difficult and time-consuming. One of the possible ways to overcome that obstacle is to present hybrid nanomaterials as an additive mixture of homogeneous NPs of the defined concentration (expressed by novel additive descriptors for the hybrid nanostructure). The simple additive scheme is already successfully applied for preliminary modeling of toxicity of conventional multiple chemicals' mixtures. 41-46

2.2.1 Modeling of joint toxicity: general approach. For the conventional organic compounds, there are four major types of modes of action in analyzing the joint toxicity of binary mixtures, *i.e.* (i) simply additive, when the ideal additive effects are observed and the joint toxic response is equal to the sum of the single chemical toxicity, (ii) more than the additive/synergism effect, when the combined effect will be greater than a sum of the toxicity of individual chemicals, (iii) less-than-additive/partial addition, when the overall toxic effect is less than a sum of the toxicity of individual chemicals, and (iv) no interaction/independent, when the joint toxic effect is equal to that

Nanoscale Paper

caused by the component with the greatest toxicity that depends on the concentration the effect may be less than additive or antagonistic. 39,40,45 According to the results reported in the literature, the most organic chemicals act jointly by simple addition. 39-42 For example, Xu and Nirmalakhandan 39 have concluded that joint effects of non-reactive chemicals are not significantly different from simple addition.³⁹ While Chen and Yeh⁴¹ have recommended that simple additivity is appropriate for preliminary modeling of toxicity of multiple chemical mixtures. Berenbaum⁴² also proposed that simple addition may be used as a universal reference for the assessment of joint effects. Based on results reported in the literature in the case of QSAR modeling for conventional organic mixtures the descriptors (C_{mix}) may be expressed by a sum of a dose/concentration of single components (C_i) in a mixture multiplied by a scaling factor (a) that accounts for the property contribution of the individual component, *i.e.* $C_{\text{mix}} = \sum_{i=1}^{n} aC_i$. According to results reported in the literature integral additive descriptors $(D_{\rm mix})$ of any individual compound may be expressed by a set of various 2D and 3D descriptors,33 and then expressed as a

 (D_{mix}) of any individual compound may be expressed by a set of various 2D and 3D descriptors, 33 and then expressed as a mole weighted average using the calculated descriptor(s) value (s) (D_n) and molar fraction of each component (R_n) as follows: $D_{\text{mix}} = R_1D_1 + R_nD_n$. 45,46 2.2.2 Additive descriptors for hybrid nanomaterials. In this

2.2.2 Additive descriptors for hybrid nanomaterials. In this study, we have proposed the modification of the methodology of internal additive descriptors for conventional mixture systems of organic compounds to express properties of hybrid nanomaterials. Thus, we have employed the methodology that is based on the assumption that the titanium oxide surface was set as constant (no descriptors), and metal cluster (s) are represented as an additive mixture of concentration-weighted descriptors for individual metals in clusters. The proposed additive calculation methodology for mixtures of compounds can be described by the following equation:

$$D_{\text{mix}} = \% \text{mol}_{\text{Me}_1} \times D_1 + \dots + \% \text{mol}_{\text{Men}} \times D_n$$
 (1)

where $D_{\rm mix}$ is the additive descriptor, *i.e.* the information on structural features of each component in the complex hybrid nanostructure translated into numerical variables; ${\rm \%mol_{Me_1}}$ – the concentration of a certain metal in the mixture; D_n – quantum chemical descriptor for the certain metal in the complex hybrid sample (expressed by a set of various 2D and 3D descriptors).

Interactions of individual chemicals in a mixture can result in synergistic or antagonistic effects as opposed to the ideal case of additive behavior *i.e.*, concentration addition (CA) and independent action (IA). To quantify the similarity degree between two systems in mixture, it is not suitable to account only for mutual or dissimilar features, but all the features of the systems have to be measured in the assessment.⁴⁷ For evaluating the similarity between two complex chemical systems the Hausdorff-like similarity measure (H_S) should be calculated.⁴⁷ The Hausdorff-like similarity measure is a function that includes information on all the elements present in the compared sets, information that is usually lost by the other

measures. The $H_{\rm S}$ is capable of equally weighing both the existence of common/comparable elements. ⁴⁷ To quantify the similarity between TiO₂-based nanomaterials modified with a mixture of noble metals, the $H_{\rm S}$ index was calculated (see ESI, Table S9†).

2.2.2 Smoluchowski equation derived descriptors. In addition to basic and additive descriptors, the sedimentation potential for metal clusters was estimated. The basic equation was derived from the Smoluchowski equation (eqn (2)) and takes into consideration the particle volume fraction of nanoparticles:⁴⁸

$$\varphi = \frac{(4/3) \cdot \pi \cdot \% \operatorname{mol}_{\operatorname{Me}_n}{}^3 \cdot (\rho - \rho_0)}{V} \cdot g \tag{2}$$

where V – the volume of solution, ρ – the mass density of the noble metal, ρ_0 – the mass density of the solvent, and g – the gravitation acceleration.

The basic equation was modified to represent complex nanomaterials: a total concentration in eqn (2) was presented as a sum of corresponding concentrations of metals in the hybrid sample. Mass density was presented as a sum of metal densities weighted in accordance with metal's concentration in the hybrid sample.

2.3 Development of nano-QSAR_{mix} models

Once a series of basic and additive descriptors for hybrid materials were generated, we built QSAR models (so-called nano-QSAR_{mix}). These models were built using Multiple Linear Regression (MLR)⁸ and Decision Tree (DT) modeling techniques. (MLR) and Decision Tree (DT) modeling techniques. (MLR) is a commonly used statistical tool for which a dependent variable (e.g., toxicity (y_i)) is expressed as a linear combination of independent variables (e.g., physicochemical properties and/or structural features ($x_1, x_2, ..., x_n$) with certain coefficients ($b_0, b_1, b_2, ..., b_n$) (eqn (3)). In this study, nano-QSAR_{mix} models were generated for the most relevant independent variables (i.e., molecular descriptors) selected by a genetic algorithm (known as MLR-GA modification). MLR models were developed using QSARINS software: 50

$$y_i = b_0 + b_1 x_1 + b_2 x_2 + b_n x_n \tag{3}$$

The Decision Tree (DT) technique is a simple and popular tool for non-linear modeling. ^{12,49,50} In the present contribution, we used a decision stump technique followed by regression meta-classifier. Each decision stump was characterized by a single attribute (descriptor). The maximal size of the decision tree was set as 4, and where the size corresponds to a number of decision stumps. Regression meta-classifier was applied to enhance the performance of decision stumps. ¹⁷ To prevent overfitting, the learning rate (shrinkage rate) was set as zero. DT modeling was performed using the machine learning environment Weka and its incorporation into the KNIME Analytics Platform. ^{52,53}

2.3.4 Quality assessment of nano-QSAR_{mix} models. All nanoparticles were split into training and validation sets. The

training set was used to build an initial model, and the validation set was used to estimate the model's predictive ability. In order to guarantee a balanced distribution, we ranged the NPs by activity and then pulled each third NP to the test set.⁴ All models were validated in accordance with recommendations of the Organization for Economic Co-operation and Development (OECD). Goodness-of-fit was accessed by the determination coefficient (R^2) and the root mean square error of calibration (RMSE_C) based on the prediction for the training set. Model's robustness (stability) was verified by internal validation using the cross-validation leave-one-out algorithm (for MLR models) or using the bagging algorithm (DF models).⁵⁰ The robustness was expressed by Q_{CV}^2 and Q_{bagging}^2 ; accordingly, root means square of cross-validation (RMSE_{CV}) also was calculated. Predictive ability of all models was assessed by the external validation coefficient (Q_{Ext}^2) , the root mean square error of prediction (RMSE_P), and Concordance Correlation Coefficient (CCC).⁵⁰ In addition, predictive performance criteria proposed by the Roy group were calculated for MLR models.^{54–56} All mentioned statistical characteristics were calculated according to the formulas summarized in the ESI (Table S6†).

The applicability domain (AD) that shows the virtual space in which the model could be applied with the optimal reliability was also assessed. In the presented work, we used a new probability-oriented distance-based approach (ADProbDist) to define the interpolation space where true and reliable predictions can be expected.⁵⁷ In addition to that, we have evaluated developed models in terms of causality as was discussed in our previous studies. 58,59

3. Results and discussion

Cytotoxicity and photocatalytic activity of the synthesized hybrid TiO2-based nanomaterials

The characterization of newly synthesized TiO2 nanomaterials modified with mono/hybrid noble metals (i.e. Ag/Au/Pd/Pt) is summarized in Table 1. The obtained hybrid nanomaterials demonstrated a high photocatalytic activity (i.e. phenol degradation in aqueous solution in the presence of visible and UV-vis radiation). At the same time, the obtained TiO2-based photocatalytic nanomaterials have shown toxic effects against Chinese hamster ovary (CHO-K1, ATCC® CCL-61TM). Both measured activities are also summarized in Table 1. As one can see, the developed TiO₂-based hybrid nanomaterials (Me_{mix}-TiO₂) demonstrated an optimized photocatalytic activity that increased with the amount of noble metals (i.e. Au/Ag/Pd/Pt) on the surface (Fig. 2, plots 2a, 2c, 2e). However, the increasing TiO2-based nanomaterial diversity resulted in increased cytotoxicity (Fig. 2, plots 2b, 2d, 2f). The relationship between the efficiency of the TiO2-based photocatalyst, the amount of noble metals in hybrid samples and their cyto-

Table 1 Hybrid TiO₂-based nanomaterial characterization

	Amount of noble metal precursor [%mol]				DETERMINE	ml o cC i o o o C o l o o o l	· PC
Sample label	Ag	Pt	Au	Pd	BET surface area [m² g ⁻¹]	The efficiency of phenol degradation [%] in UV-vis light	pEC ₅₀ [mol mL ⁻¹]
Pure TiO ₂	0.0	0.0	0.0	0.0	_	63.6	5.52
0.1Ag	0.1	0.0	0.0	0.0	61.0	61.8	5.60
0.5Ag	0.5	0.0	0.0	0.0	91.0	64.4	5.83
1.5Ag	1.5	0.0	0.0	0.0	89.0	70.3	6.23
2.5Ag	2.5	0.0	0.0	0.0	91.0	73.5	6.76
4.5Ag	4.5	0.0	0.0	0.0	67.5	73.5	7.40
0.1Ag_0.1Au	0.1	0.0	0.1	0.0	106.5	63.0	5.67
0.5Ag_0.1Au	0.5	0.0	0.1	0.0	112.0	52.9	6.25
1.5Ag_0.1Au	1.5	0.0	0.1	0.0	90.2	65.6	6.58
2.5Ag_0.1Au	2.5	0.0	0.1	0.0	79.0	60.0	6.80
0.1Ag_0.5Au	0.1	0.0	0.5	0.0	103.0	51.4	6.05
2.5Ag_0.5Au	2.5	0.0	0.5	0.0	90.4	64.6	7.01
4.5Ag_0.5Au	4.5	0.0	0.5	0.0	111.4	69.5	7.41
0.1Ag_0.1Pt	0.1	0.1	0.0	0.0	92.0	85.4	5.92
0.5Ag_0.1Pt	0.5	0.1	0.0	0.0	94.0	68.4	6.29
1.5Ag_0.1Pt	1.5	0.1	0.0	0.0	145.6	85.6	6.63
2.5Ag_0.1Pt	2.5	0.1	0.0	0.0	86.0	71.1	7.07
0.1Ag_0.5Pt	0.1	0.5	0.0	0.0	112.5	96.8	5.97
2.5Ag_0.5Pt	2.5	0.5	0.0	0.0	119.0	96.1	7.10
0.1Ag_0.1Pd	0.1	0.0	0.0	0.1	79.0	77.4	5.56
0.5Ag_0.1Pd	0.5	0.0	0.0	0.1	77.5	72.1	6.46
1.5Ag_0.1Pd	1.5	0.0	0.0	0.1	98.0	96.0	6.76
2.5Ag_0.1Pd	2.5	0.0	0.0	0.1	98.0	94.9	7.20
0.1Ag_0.5Pd	0.1	0.0	0.0	0.5	115.0	99.2	5.70
2.5Ag_0.5Pd	2.5	0.0	0.0	0.5	107.0	99.5	6.88
0.1Ag_0.1Pt_0.1Au	0.1	0.1	0.1	0.0	94.0	84.4	5.88
0.1Pt_0.1Au_0.1Pd	0.0	0.1	0.1	0.1	92.0	100.0	5.92
0.1Ag_0.1Pt_0.1Pd	0.1	0.1	0.0	0.1	89.0	100.0	5.86
0.1Ag_0.1Au_0.1Pd	0.1	0.0	0.1	0.1	85.0	92.8	5.88
0.1Ag_0.1Pt_0.1Au_0.1Pd	0.1	0.1	0.1	0.1	94.0	100.0	6.02

Nanoscale Paper

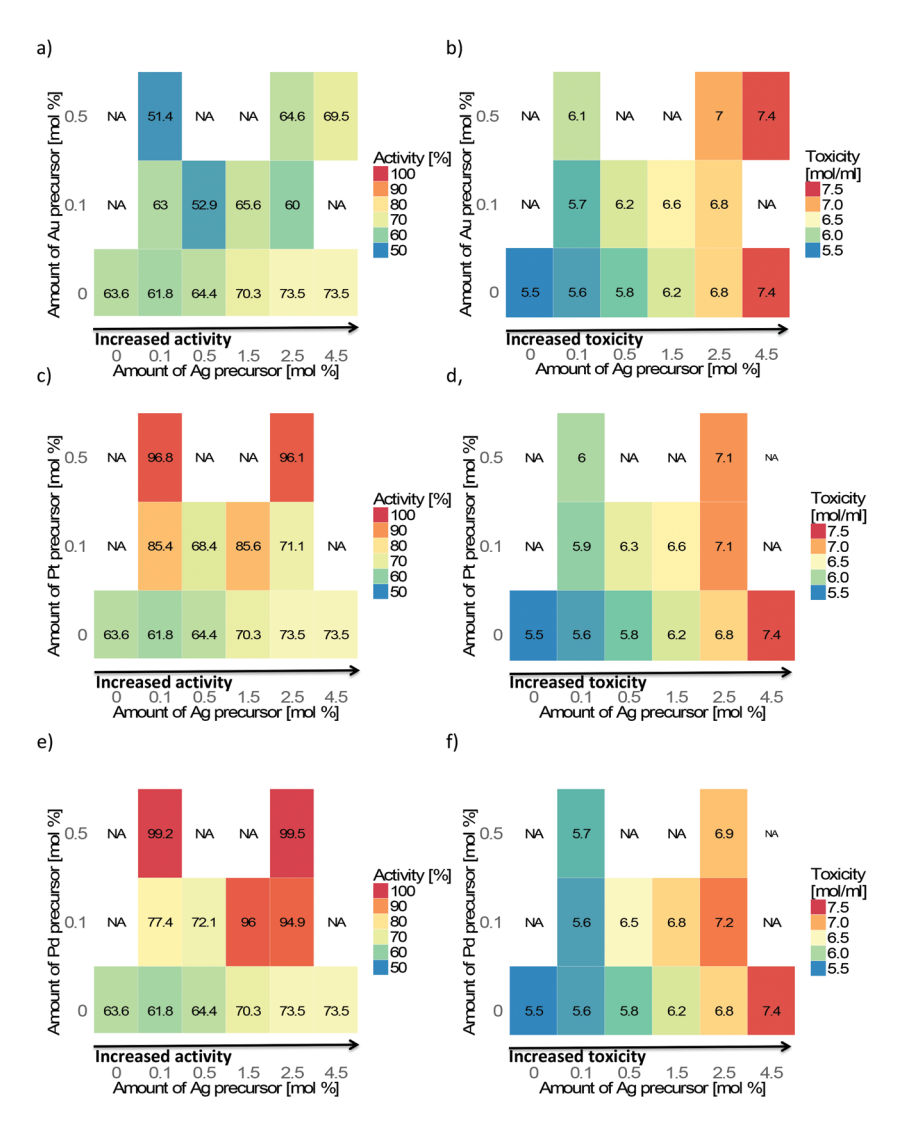


Fig. 2 Concentration-dependent photocatalytic activity and toxicity related to mixed concentration of noble metals, i.e. (a, b) Ag/Au, (c, d) Pt/Ag, (e, f) Pd/Ag, respectively.

toxicity effect is shown in Fig. 2, Table 1. We observed that the photocatalytic activity (Fig. 2, plots 2a, 2c, 2d) and the cytotoxicity (Fig. 2, plots 2b, 2d, 2f) of hybrid TiO₂-based nanomaterials grow with an increasing amount of Ag. At the same time, both cytotoxicity and photocatalytic activity change depending on the type and concentration of the second Au metal (Fig. 2). Among tri- and four metallic nanostructures, the cytotoxicity changed in the row: Ag-Pt-Pd < Ag-Au-Pd ~ Ag-Pt-Au < Ag-Pt-Au-Pd. The replacement of Pt or Pd with Au slightly increased the cytotoxicity. At the same time, there was no statistically significant difference if Au is combined with either Pt or Pd (Table 1). Interestingly, there was no considerable difference in photocatalytic properties of tri- and four metallic nanostructures (Table 1).

3.1.1 Predictive Nano-QSPR_{mix} models for phenol degradation. In order to design efficient and safe hybrid TiO₂-based nanostructures, we developed predictive models as described in the Materials and methods section. In the case of photo-

catalytic properties, potential MLR-GA models were statistically inadequate. In contrast, the nonlinear DT model was of high quality. This model is characterized with $R_{\rm adj}^2$ = 0.82, RMSE_C = 5.99, $Q_{\text{bagging}}^2 = 0.81$, RMSE_{CV} = 8.76, $Q_{\text{EXT}}^2 = 0.80$, and $RMSE_P = 6.48$. Fig. 3 represents the graphical form of the DT model. The applicability domain (AD) is represented in Fig. 3. According to the AD, all nanostructures are within the AD (of $\pm 3\sigma$), four compounds (i.e. 4.5Ag_0.5Au, 2.5Ag_0.5Pt, 1.5Au_0.1Pt, 0.1Ag_0.5Pt) are located in the boundary of the inner (i.e. orange) confidence ellipse, which corresponds to 99 percent confidence intervals, it appears to be inside the AD and its model-based prediction should be therefore considered reliable. The DT model includes four descriptors: the amount of Pd in the sample (%mol_{Pd}), sedimentation potential of Pt clusters (φ_{Pt}) , additive sedimentation potential of samples (φ_{mix}) , and BET surface area (BET_{area}). Values of descriptors and the decision stumps are summarized in the ESI (Tables S1, S2 and S6†).

Paper Nanoscale

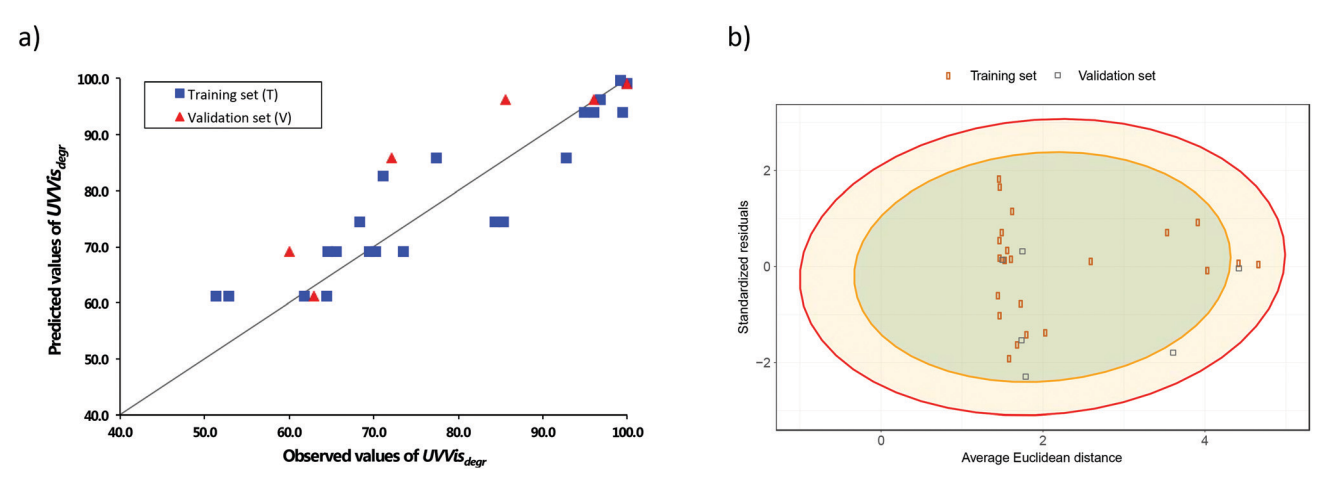


Fig. 3 (a) Observed-predicted diagram of the DT model for photocatalytic activity; (b) applicability domain for the DT model for photocatalytic activity.

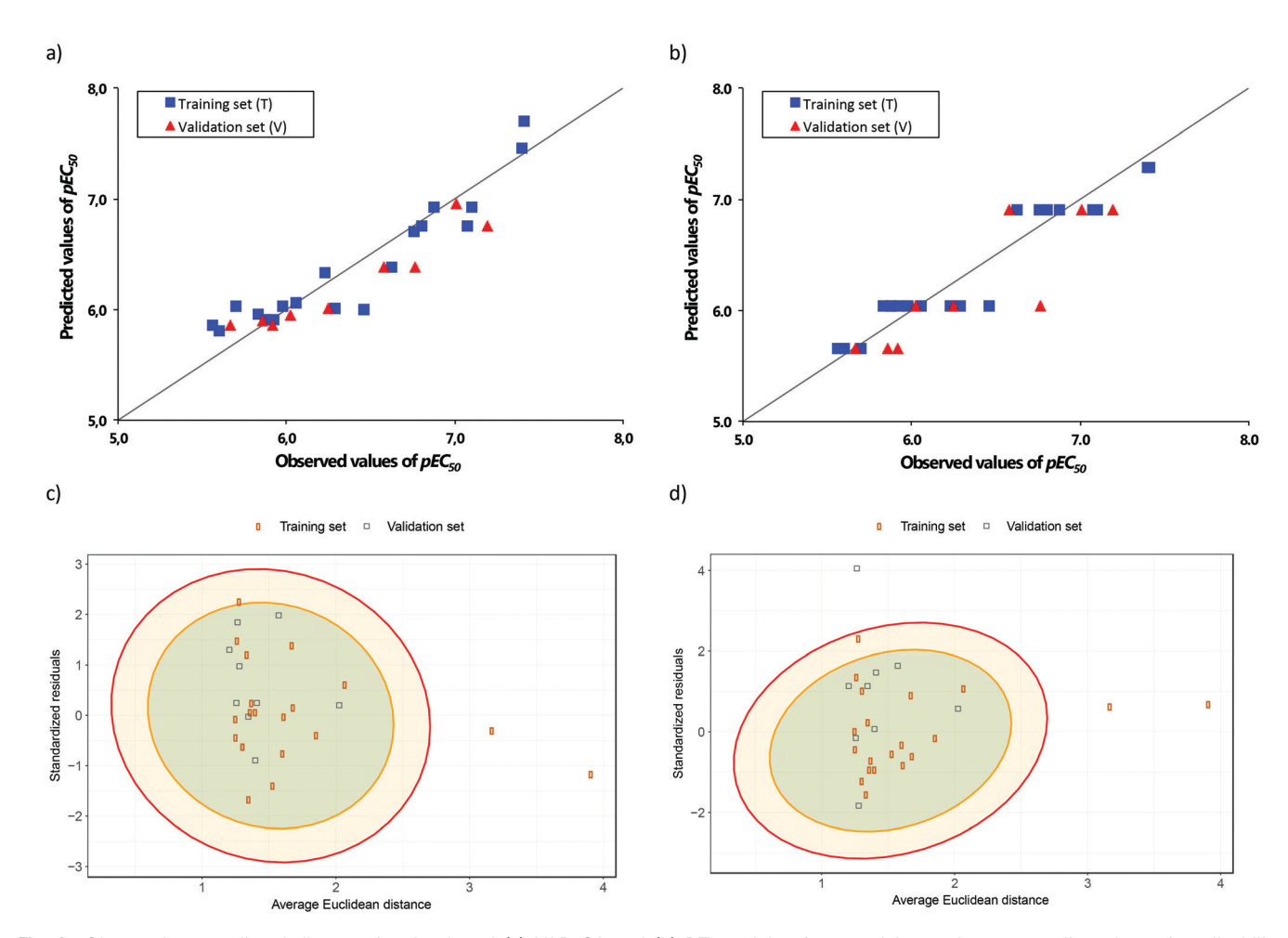


Fig. 4 Observed vs. predicted diagram for developed (a) MLR-GA and (b) DT models of cytotoxicity; and corresponding plots of applicability domains: (c) for MLR-GA, and (d) for the DT model.

3.1.2 Predictive Nano-QSAR_{mix} models for cytotoxicity. Both linear MLR-GA and non-linear DT models successfully described the cytotoxicity of NPs. Observed-predicted plots, as well as applicability domain areas of the nano-QSAR_{mix} models for cytotoxicity, are presented in Fig. 4. Statistical characteristics of developed models are presented in Table 2.

Nanoscale

Table 2 Statistics for developed nano-QSAR_{mix} models for the cytotoxicity effect

	MLR-GA model	DT model
$R_{\rm adj}^2$	0.87	0.90
$RMSE_C$	0.20	0.17
$Q_{\rm int}^2/Q_{\rm bagging}^2$	0.84	0.74
RMSE _{CV}	0.23	0.22
${ m RMSE}_{ m CV} \ {Q_{ m EXT}}^2$	0.80	0.90
RMSE _P	0.19	0.16

The MLR-GA model was additionally characterized with the following statistical parameters: $MAE_{tr} = 0.16$, $CCC_C = 0.93$, $MAE_{cv} = 0.18$, $CCC_{CV} = 0.92$, $MAE_{EXT} = 0.19$, $CCC_{EXT} = 0.87$, k = 0.190.97, k' = 1.02, $R^2 Y_{\text{scr}} = 0.05$, $Q^2 Y_{\text{scr}} = -0.18$, and F = 124.54.

The developed MLR-GA model (Fig. 4a) utilized the descriptor that represents additive electronegativity (χ_{mix}):

$$pEC_{50} = 6.37(\pm 0.07) + 0.56(\pm 0.02) \cdot \chi_{mix}$$
 (4)

The obtained DT model was based on one descriptor that characterized electron affinity (A). The decision stumps are summarized in the ESI (Table S3†). Despite the better statistical characteristics (Fig. 4e), this model has a lower quality than the MLR-GA model (eqn (4)). As it can be seen from Fig. 4a and e, the DT model does not properly differentiate activities, providing discrete predictions. Values of selected descriptors, predicted, and observed cytotoxicity are presented in Table S4.† The AD plot for both models (Fig. 4c and d) demonstrated that two compounds of the training set (i.e. TiO2 loaded with 4.5Ag and 4.5Ag_0.5Au) are located outside of $\pm 3\sigma$ and should be treated with caution as its prediction might potentially be less accurate whereas a chemical that falls outside the defined limits of the model's reliable predictions (i.e. outside the orange zone).⁵⁷ Thus, we can assume that 4.5Ag and 4.5Ag_0.5Au NPs are structurally different from the other training compounds and are, thus, deliberated as outliers in the structural domain of the model. Indeed, this conclusion becomes obvious considering the fact that these compounds had the highest values of both descriptors (i.e. χ_{mix} and A, ESI, Table S4†) among all compounds in the training set. However, these were found to have relatively small residual errors (that did not fall outside the limits of ±3 of the standard deviations) (ESI, Table S4†). The samples 4.5Ag and 4.5Ag_0.5Au NPs thus might be considered as good high leverage points (also called the structurally influential outlier) that stabilized the model.⁵⁷ However, its prediction should be treated with the utmost caution. In addition, the AD has been verified by the plot of standardized cross-validated residuals versus leverages (Williams plot) (ESI, Fig. S2†).60 In order to alleviate chance correlation, and evaluate the significance of the developed Nano-QSAR_{mix} model, the Y-randomization test (so-called Y-scrambling test) was additionally performed. 61 We built 2000 models (so-called "random models") utilizing the same descriptor (χ_{mix}) but correlated with cytotoxicity pEC_{50} data randomly shuffled every time. Based on the calculations of the $R^2Y_{\rm scr}$ and $Q^2Y_{\rm scr}$ values for these models we were able to determine the minimal error that can be calculated without the presence of any model. Since the values of R^2Y_{scr} were about 17 times lower than those for the Nano-QSAR_{mix} model and the value of Q^2Y_{scr} was negative (Table S8, Fig. S1, ESI†), we have confirmed the significance of the developed Nano-QSAR_{mix} (eqn (4)).

3.2 Interpretation of nano-QSAR_{mix} models

In order to understand the relationship between mechanisms of cytotoxicity and photocatalytic activity of hybrid TiO2-based nanomaterials, we cross-analyzed the developed nano-QSARmix models. We suggest that the developed models prove that the increased cytotoxicity, as well as the photocatalytic activity, is referred to the h^+/e^- pair generation (eqn (5)-(11)).^{3,21,26} As we demonstrated in our previous studies^{1,4} the presence of noble metals may result in increased photocatalytic activity because of: (i) extended absorption in visible light due to the localized surface plasmon resonance (LSPR) that causes transfer of photo-excited electrons (e-) from the noble metal to the conduction band of the TiO2 surface; or (ii) charge separation mechanism in UV-vis light when the noble metal traps photogenerated charge pairs (i.e. electrons (e⁻) and holes (h⁺)) that results in lengthening of its lifetime and leads to reduced charge recombination and facilitates the transport of photogenerated electrons (e⁻) to the TiO₂ surface (Fig. 5).^{20,22,24,25}

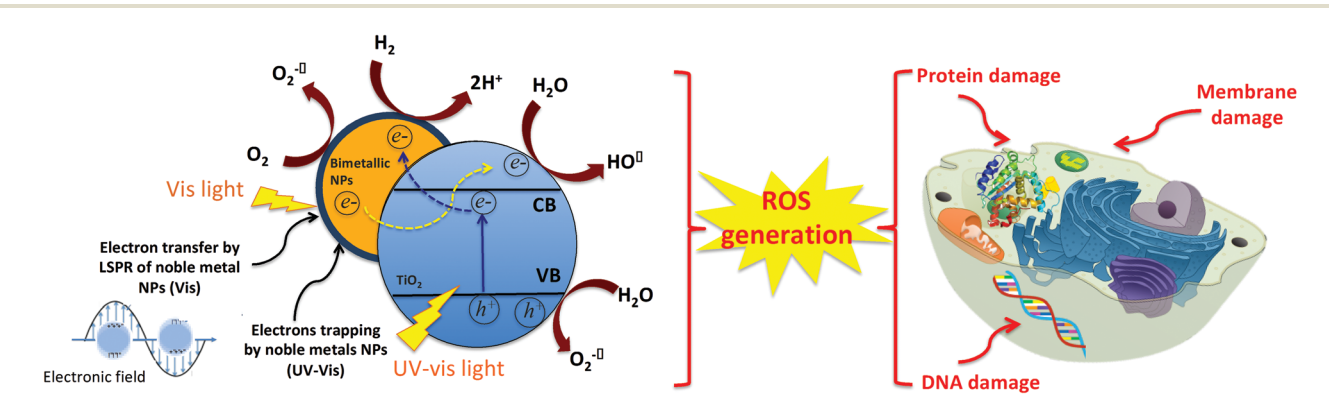


Fig. 5 Schematic illustration of semiconductor excitation by vis and UV-vis light, charge carriers' generation, ROS production, and cell damage.

Paper Nanoscale

Consequently, in both mechanisms photo-generated h⁺/e⁻ pairs cause besides indirect oxidation and reduction processes that are carried out by reactive oxygen species (ROS), Fig. 5.^{1,3}

At the same time, ROS production is the most common toxicity cause as discussed in the literature in the case of nanoparticles. 4,9,11 Based on our previous results we have indicated that the main photogenerated ROS include singlet oxygen (¹O₂), superoxide (*O₂), hydroxyl radicals (*OH), hydroperoxyl radical (*O₂H) and hydrogen peroxide (H₂O₂). The high efficiency of surface modified TiO2-based semiconductors can be attributed to the involvement of TiO_2 band gap (E_{α}) excitation and absence of noble metals at the TiO2 surface. It can be expected that noble metals (i.e. Pd/Pt) because of LSPR may trap holes (h⁺), at the same time photo-generated electrons can be then transferred from the valence band to the conduction band of TiO2 and to its surface where redox processes were initiated (Fig. 5a). ^{1,3,23} Thus, observed reduction of the electron-hole pair recombination influences the reactive oxygen species (ROS) formation and the photocatalytic redox process initiation (eqn (5)-(11)).3,21,26

$$Me_{mix}$$
-TiO₂ $(V_O^+) \xrightarrow{h\nu(UV-vis)} Me_{mix}(LSPR \bar{e})TiO_2(V_O^+)$ (5)

$$\begin{aligned} & Me_{mix}(LSPR\bar{e})TiO_{2}(V_{O}^{+}) + 2H^{+} \\ & \rightarrow Me_{mix} - TiO_{2}(V_{O}^{+}) + H_{2} \end{aligned} \tag{6}$$

$$Me_{mix}$$
- $TiO_2 \xrightarrow{h\nu(UV-vis)} Me_{mix}$ - $TiO_2(CB \bar{e})$ (7)

$$Me_{mix}\text{-TiO}_2(CB\bar{e}) \rightarrow Me_{mix}\text{-TiO}_2 + H_2 \tag{8}$$

$$Me_{mix}(LSPR\bar{e})TiO_2 \rightarrow Me_{mix}-TiO_2(CB\bar{e})$$
 (9)

$$Me_{mix}$$
-TiO₂(CB \bar{e}) + H₂O \rightarrow OH' (10)

$$OH' + pollutant \rightarrow degraded product$$
 (11)

Results obtained from developed models (models for both UV-vis_{degr} and pEC50, eqn (4)) indicated that the mechanisms of photocatalysis under UV-vis light (UV-vis_{degr}) and the cytotoxicity effect (pEC50) share similar causes (Fig. 5). First, the developed DT model for phenol degradation under UV-vis light irradiation clearly indicates that the presence of Pd and Pt at the surface of TiO2 significantly influences the degradation (expressed by %mol_{Pd}, φ_{Pt} , φ_{mix} , and BET_{area} descriptors, see Fig. 3, Table S2, ESI†), on comparing with the presence of Au or Ag on the TiO2 surface. Next, we have shown that the cytotoxicity of hybrid TiO₂-based nanomaterials (eqn (4)) is related to additive electronegativity (χ_{mix}) and electron affinity (A) of studied nanomaterials (eqn (4)) that are indirectly related to the electron generation and ROS formation. Since the electronegativity was positively correlated with the cytotoxicity (+0.19 χ_{mix} , eqn (12)) and increases in the row Au (2.54) > Pt (2.28) > Pd (2.20) > Ag (1.93), it can be expected that some ions (in presented case - ions of silver) are released from the TiO₂ surface easier than others (Fig. 5b):

$$\gamma \approx \gamma_{\text{cation}} + 3.36.$$
 (12)

This could be directly linked to the observed Ag related concentration-dependent increase of toxicity in samples (Fig. 2). A

similar observation was made by Li et al. 28,29 and Beer et al. 30 who have shown that Ag-TiO2 NPs generally exhibit stronger cytotoxicity than TiO2 NPs. Next, the cytotoxicity increases as electron affinity (A) of a sample increases (Fig. 4b). In fact, the released metal ions may induce the formation of ROS, and damage the integrity of the cell, as well as structures of proteins or DNA inside the cell (Fig. 5). 9,27 Obtained results indicate that cytotoxicity of hybrid TiO2-based nanoparticles linearly changes with the concentration, and nonlinearly changes in terms of additive parameters making individual properties of each metal in the sample extremely important. In our earlier work^{1,31} the influence of the bimetallic structure on both photocatalytic and cytotoxicity properties was highlighted. In this regard, the current report presents an extension of that study, as bimetallic (hybrid) nanomaterials are analyzed together with hybrid tri- and tetra-metallic samples.

4. Conclusion

In this work, a series of hybrid nanoparticles was investigated using experimental and computational modeling techniques. To improve the photocatalytic performance of TiO₂ nanomaterials, surface modifications with noble Au/Ag/Pd/Pt metals were introduced during the synthesis. We discussed then hybrid TiO₂-based nanostructures in the context of cytotoxicity and photocatalysis.

For the first time, the developed additive descriptor methodology was tested for novel two-, tri- and tetra-metallic hybrid TiO₂-based photocatalysts. Based on developed quantitative structure-activity/property relationship models and experimental evidence we described the contribution of physicochemical factors of investigated nanoparticles that influence their photocatalytic properties and environmental toxicity. We demonstrated that cytotoxicity is related to photocatalytic properties of multicomponent TiO2-based samples. We have found the following parameters that play a crucial role in the cell damage are: (i) the content of silver vs. gold/palladium/platinum, (ii) solubility, (iii) the electronic properties of a sample (band gap and conduction band energy level) and (iv) photocatalytic activity. Knowledge of physicochemical characteristics that contribute to toxicity is essential for hybrid nanomaterial's safer-by-design development.

The proposed approaches allow the control of features of electron structure and electron transfer in nanomaterials, making them suitable for *safer-by-design* nanomaterials' development. The presented modeling approach is a good starting point in the design and synthesis of efficient multi-component TiO₂-based photocatalysts with reduced cytotoxicity against eukaryotic cells.

Author contributions

T.P, B.R, and A.M supervised and directed the project. A.M. conceived the concept; A.M. designed the research, analyzed

Nanoscale Paper

the experimental data and prepared discussion; A.M., performed the computational part and prepared the manuscript; E.M, A. Malankowska performed the experimental data. N.S. calculated descriptors derived from Smoluchowski equation. All authors took part in editing and have given approval to the final version of the manuscript.

Conflicts of interest

The authors declare no competing financial interest.

Acknowledgements

The researcher gratefully acknowledges support from the National Science Center (no. 2015/19/N/NZ7/01593) and Horizon 2020 EU (no. 814426). This work was also supported in part by the National Science Foundation through the CHE-1800476 Award and ND EPSCOR Award #IIA-1355466.

References

- A. Mikolajczyk, A. Malankowska, G. Nowaczyk, A. Gajewicz,
 S. Hirano, S. Jurga, A. Zaleska-Medynska and T. Puzyn,
 Environ. Sci.: Nano, 2016, 3, 1425–1435.
- 2 S. Lin, T. Yu, Z. Yu, X. Hu and Y. Yin, *Adv. Mater.*, 2018, 30, 1705691.
- 3 A. Zielińska-Jurek, J. Nanomater., 2014, 3, 1-17.
- 4 A. Mikolajczyk, A. Gajewicz, E. Mulkiewicz, B. Rasulev, M. Marchelek, M. Diak, S. Hirano, A. Zaleska-Medynska and T. Puzyn, *Environ. Sci.: Nano*, 2018, 5, 1150–1160.
- 5 E. Burello, Environ. Sci.: Nano, 2016, 2, 454-462.
- 6 I. Lynch, C. Weiss and E. Valsami-Jones, *Nano Today*, 2014, 9, 266–270.
- 7 I. V. Tetko, O. Engkvist and H. Chen, *Future Med. Chem.*, 2016, **8**, 1801–1806.
- 8 T. Puzyn, B. Rasulev, A. Gajewicz, X. Hu, T. P. Dasari, A. Michalkova, H. M. Hwang, A. Toropov, D. Leszczynska and J. Leszczynski, *Nat. Nanotechnol.*, 2011, **6**, 175–178.
- 9 A. Gajewicz, N. Schaeublin, B. Rasulev, S. Hussain, D. Leszczynska, T. Puzyn and J. Leszczynski, *Nanotoxicology*, 2014, 9, 1–13.
- 10 A. Mikolajczyk, A. Gajewicz, B. Rasulev, N. Schaeublin, E. Maurer-Gardner, A. S. Hussain, J. Leszczynski and T. Puzyn, *Chem. Mater.*, 2015, 27, 2400–2407.
- 11 E. Burello and A. P. Worth, Nanotoxicology, 2011, 5, 228–235.
- 12 F. Luan, V. V. Kleandrova, H. González-Díaz, J. M. Ruso, A. Melo, A. Speck-Planche and M. N. Cordeiro, *Nanoscale*, 2014, 6, 10623–10630.
- 13 V. V. Kleandrova, F. Luan, H. González-Díaz, J. M. Ruso, A. Speck-Planche and M. N. Cordeiro, *Environ. Sci. Technol.*, 2014, 48, 14686–14694.
- 14 V. V. Kleandrova, F. Luan, H. González-Díaz, J. M. Ruso, A. Melo, A. Speck-Planche and M. N. Cordeiro, *Environ. Int.*, 2014, 73, 288–294.

15 M. González-Durruthy, S. Manske Nunes, J. Ventura-Lima, M. A. Gelesky, H. González-Díaz, J. M. Monserrat, R. Concu and M. N. Cordeiro, J. Chem. Inf. Model., 2019, 59, 86–97.

- 16 M. González-Durruthy, J. M. Monserrat, P. Viera de Oliveira, S. B. Fagan, A. V. Werhli, K. Machado, A. Melo, H. González-Díaz, R. Concu and M. N. Cordeiro, *Chem. Res. Toxicol.*, 2019, 32, 566–577.
- 17 M. González-Durruthy, J. M. Monserrat, B. Rasulev, G. M. Casañola-Martín, J. M. Barreiro Sorrivas, S. Paraíso-Medina, V. Maojo, H. González-Díaz, A. Pazos and C. R. Munteanu, *Nanomaterials*, 2017, 7, E386.
- 18 M. González-Durruthy, A. V. Werhli, V. Seus, K. S. Machado, A. Pazos, C. R. Munteanu, H. González-Díaz and J. M. Monserrat, Sci. Rep., 2017, 7, 13271.
- 19 I. Olier, N. Sadawi, G. R. Bickerton, J. Vanschoren, C. Grosan, L. Soldatova and R. D. King, *Mach. Learn.*, 2018, 107, 285–311.
- 20 A. Zielinska-Jurek and A. Zaleska, *Catal. Today*, 2014, 230, 104–111.
- 21 I. Chanu, P. Krishnamurthi and P. T. Manoharan, *J. Phys. Chem. C*, 2017, **121**, 9077–9088.
- 22 M. Klein, J. Nadolna, A. Gołąbiewska, P. T. Mazierski, T. Klimczuk, H. Remita and A. Zaleska-Medynska, *Appl. Surf. Sci.*, 2016, 378, 37–48.
- 23 A. Cybula, J. B. Priebe, M.-M. Pohl, J. W. Sobczak, M. Schneider, A. Zielinska-Jurek, A. Bruckner and A. Zaleska, Appl. Catal., B, 2014, 152, 202–211.
- 24 I. H. Chanu, L. R. Devi, N. Khumanthem, N. I. Singh, D. Kumar and O. M. Sungh, *Russ. J. Bioorg. Chem.*, 2017, 43, 177–185.
- 25 Z. Y. Zhang, Z. Wang, S. W. Cao and C. Xue, *J. Phys. Chem. C*, 2013, **117**, 25939–25947.
- 26 R. K. Shukla, V. Sharma, S. Pandey, S. Singh, S. Sultana and A. Dhawan, *Toxicol. in Vitro*, 2011, 25, 231–241.
- 27 M. Ema, H. Okuda, M. Gamo and K. A. Honda, *Reprod. Toxicol.*, 2017, 67, 149–164.
- 28 M. Li, M. E. Noriega-Trevino, N. Nino-Martinez, C. Marambio-Jones, J. Wang, R. Damoiseau, F. Ruiz and V. Hoek, *Environ. Sci. Technol.*, 2011, 241, 8989–8995.
- 29 Y. Li, W. Zhang, J. Niu and Y. Chen, ACS Nano, 2012, 6, 5164-5165.
- 30 C. Beer, R. Foldbjerg, Y. Hayashi, D. S. Sutherland and H. Autrup, *Toxicol. Lett.*, 2012, 208, 286–292.
- 31 A. Mikolajczyk, N. Sizochenko, E. Mulkiewicz, A. Malankowska, M. Nischk, P. Jurczak, S. Hirano, G. Nowaczyk, A. Zaleska-Medynska, J. J. Leszczynski and T. Puzyn, *Beilstein J. Nanotechnol.*, 2017, 8, 2171–2180.
- 32 A. Fracanzani, S. Petta, R. Lombardi, G. Pisano, M. Russello, D. Consonni, C. Di Marco, C. Camma, L. Mensi, P. Pongiovann, L. Valenti, S. Craxi and S. Farion, Clin. Gastroenterol. Hepatol., 2017, 15, 1604–1611.
- 33 Molecular Descriptors for Chemoinformatics, ed.R. Todeschini and V. Consonni, Wiley-VCH, 2009.
- 34 C. E. Rasmussen and C. K. Williams, *Gaussian Processes for Machine Learning*, 2006.
- 35 GaussView version 3.0, Gaussian Inc., Pittsburgh PA., 2003.

Paper

36 M. J. S. Frisch, G. E. Scuseria, M. A. Robb, J. R. Cheeseman, G. Scalmani, V. Barone, B. Mennucci, G. A. Petersson, H. M. Nakatsuji, M. Caricato, X. Li, H. P. Hratchian, A. F. Izmaylov, J. Bloino, G. Zheng, J. L. Sonnenberg, M. Hada, M. K. Ehara, K. Toyota, R. Fukuda, J. Hasegawa, M. Ishida, T. Nakajima, Y. Honda, O. Kitao, H. Nakai, T. Vreven, J. A. Montgomery, J. E. Peralta, F. Ogliaro, M. J. Bearpark, J. Heyd, E. N. Brother, K. N. Kudin, Staroverov, R. Kobayashi, J. Normand, K. Raghavachari, A. P. Rendell, J. C. Burant, S. S. Iyengar, J. Tomasi, M. Cossi, N. Rega, N. J. Millam, M. Klene, J. E. Knox, J. B. Cross, V. Bakken, C. Adamo, J. Jaramillo, R. Gomperts, R. E. Stratmann, O. Yazyev, A. J. Austin, R. Cammi, C. Pomelli, J. W. Ochterski, R. L. Martin, K. Morokuma, V. G. Zakrzewski, G. A. Voth, P. Salvador, J. J. Dannenberg, S. Dapprich, A. D. Daniels, A. Farkas, J. B. Foresman, J. V. Ortiz, J. Cioslowski and D. Fox, Gaussian 09, Gaussian, Inc., Wallingford, CT, USA, 2009.

- 37 J. P. Perdew, K. Burke and Y. Wang, *Phys. Rev. B: Condens. Matter Mater. Phys.*, 1996, 54, 16533–16539.
- 38 J. P. Perdew, K. Burke and M. Ernzerhof, *Phys. Rev. Lett.*, 1996, 77, 3865.
- 39 S. Xu and N. Nirmalakhandan, Water Res., 1998, 32, 2391– 2399.
- 40 R. Altenburger, H. Walter and M. Grote, *Environ. Sci. Technol.*, 2004, **38**, 6353–6362.
- 41 C.-Y. Chen and J.-T. Yeh, *Environ. Toxicol. Water Qual.*, 1996, 11, 83–90.
- 42 M. C. Berenbaum, J. Theor. Biol., 1985, 114, 413-431.
- 43 L. T. Qin, Y. H. Chen, H. Zhang, L. Y. Mo, H. H. Zeng and Y. P. Liang, *Chemosphere*, 2018, **198**, 122–129.
- 44 P. Polishchuk, T. Madzhidov, T. Gimadiev, A. Bodrov, R. Nugmanov and A. Varnek, *J. Comput.-Aided Mol. Des.*, 2017, 31, 829–839.
- 45 R. Altenburger, M. Nendza and G. Schuurmann, *Environ. Toxicol. Chem.*, 2003, 22, 1900–1915.

- 46 E. N. Muratov, E. V. Varlamova, A. G. Artemenko, P. G. Polishchuk and V. E. Kuz'min, Mol. Inf., 2012, 31, 202–221.
- 47 A. Mauri, D. Ballabio, R. Todeschini and V. Consonni, *J. Chemoinf.*, 2016, **8**, 49.
- 48 D. F. Calef and P. G. Wolynes, J. Chem. Phys., 1983, 78, 4145–4153.
- 49 J. Devillers, Genetic Algorithms in Molecular Modeling, Academic Press, 1996.
- 50 P. Gramatica, N. Chirico, E. Papa, S. Cassani and S. Kovarich, J. Comput. Chem., 2013, 34, 2121–2132.
- 51 I. Ponzoni, V. Sebastian-Perez, C. Reguena-Triguero, C. Roca, M. J. Martinez, F. Cravero, M. F. Diaz, J. A. Paez, R. Arrayas, G. J. Adrio and N. E. Campillo, *Sci. Rep.*, 2017, 7, 2403.
- 52 C. Ma, L. Wang and X. Q. Xie, *J. Chem. Inf. Model.*, 2011, 51, 521–531.
- 53 M.-L. Lee, I. Aliagas, J. A. Feng, T. Gabriel, T. J. O'Donnell, B. S. Sellers, B. Wiswedel and A. Gobbi, *I. Cheminf.*, 2017, 9, 38.
- 54 K. Roy, S. Kar and P. Ambure, *Chemom. Intell. Lab. Syst.*, 2015, 145, 22-29.
- 55 K. Roy and S. Kar, *In Silico Methods for Predicting Drug Toxicity*, 2015, vol. 2, pp. 71–120.
- 56 K. Roy, R. N. Das, P. Ambure and R. B. Aher, *Chemom. Intell. Lab. Syst.*, 2016, 52, 18–33.
- 57 A. Gajewicz, Environ. Sci.: Nano, 2018, 5, 408-421.
- 58 N. Sizochenko, A. Gajewicz, J. Leszczynski and T. Puzyn, *Nanoscale*, 2016, 8, 7203–7208.
- 59 N. Sizochenko, B. Rasulev, A. Gajewicz, V. Kuz'min, T. Puzyn and J. Leszczynski, *Nanoscale*, 2014, 6, 13986– 13993.
- 60 F. Sahigara, K. Mansouri, D. Ballabio, A. Mauri, V. Consonni, R. K. Todeschini and A. Tropsha, *Molecules*, 2012, 17, 4791–4810.
- 61 S. Zhang, A. Golbraikh, S. Oloff, H. Kohn and A. Tropsha, J. Mol. Graphics Modell., 2006, 46, 1984–1995.